LA-UR-16-26696
Approved for public release; distribution is unlimited.

Title: Arbitrary Order Mixed Mimetic Finite Differences Method with Nodal Degrees of Freedom

Author(s): Iaroshenko, Oleksandr
Gyrya, Vitaliy
Manzini, Gianmarco

Intended for: Report

Issued: 2016-09-01

Arbitrary Order Mixed Mimetic Finite Differences Method with Nodal Degrees of Freedom

Oleksandr Iaroshenko, Vitaliy Gyrya, Gianmarco Manzini

August 31, 2016

1 Introduction

In this work we consider a modification to an arbitrary order mixed mimetic finite difference method (MFD) for a diffusion equation on general polygonal meshes [1]. The modification is based on moving some degrees of freedom (DoF) for a flux variable from edges to vertices. We showed that for a non-degenerate element this transformation is locally equivalent, i.e. there is a one-to-one map between the new and the old DoF. Globally, on the other hand, this transformation leads to a reduction of the total number of degrees of freedom (by up to 40%) and additional continuity of the discrete flux.

In this work we will follow the Mimetic Finite Difference method construction that is largely similar to that of Finite Element methods in the sense that it follows the same steps. It starts of with rewriting the PDE in a weak form. Elements of the approximation spaces are represented in terms of their DoFs, which are associated with vertices, edges and the area of the elements. The bilinear forms corresponding to the integrals of products of functions arising in the weak formulation in the discrete settings are represented by matrices that are built element by element and then assembled into their global form.

Since for non-degenerate elements there is a one-to-one map between the new and old DoF for the flux variable we were able to build a prototype of the new method based on the old one [1] simply by inserting this transformation matrix locally. Testing the prototype method on non-degenerate meshes we verified that it has the same order of convergence as the previous method [1], but now with additional benefits of fewer DoF. Henceforth, we made built and implemented the original construction (not based on the transformation from the old construction) for the necessary blocks (to be discussed later in details) and tested on wide range of meshes. These meshes included degenerate elements (e.g. hanging nodes) both on and away from the boundary. In all cases the new method showed the same convergence rate as the previous method for problems with continuous diffusion tensor coefficient.

A number of experiments with discontinuous diffusion coefficient demonstrated that in order to obtain higher order of convergence the mesh has to conform to the discontinuity. For such meshes the previous method did retain the same convergence rate (as for continuous diffusion coefficient) while the new method did not. This happens due to the added continuity in the tangential component of the discrete flux variable at the interface vertices. This continuity is generally not present in the continuous solution. We are presently investigating a remedy based on additional DoF for the interface vertices that would correspond to the jump in the tangential component of the flux. The preliminary results are very promising.

The rest of the report is organized as follows. In section 2 we present a more detailed outline of the construction. In section 3 we present the discretizations of the bilinear form discussed in section 2. In section 4 we present various numerical tests for the new method and the comparison with the previous method. Finally, in section 5 we make several concluding remarks.

2 Outline of the mixed mimetic finite difference discretization

We consider a steady state diffusion problem

$$\operatorname{div}(K\nabla p) = -f \qquad \text{in } \Omega \subset \mathbb{R}^2 \tag{1}$$

with appropriate boundary conditions, e.g. Dirichlet boundary conditions $p = g$ on $\partial\Omega$. Here K is a symmetric diffusion tensor that may vary in space. We will assume it to be uniformly elliptic.

The mixed formulation of (1) is based on the introduction of a new variable $\mathbf{u}$ for the flux and rewrite (1) as a first order system for $\mathbf{u}$ and p:

$$\mathbf{u} = -K\nabla p \qquad \text{in } \Omega, \tag{2}$$

$$\operatorname{div} u = f \qquad \text{in } \Omega, \tag{3}$$

$$p = g \qquad \text{on } \partial\Omega. \tag{4}$$

The MFD construction, just like the Finite Element (FE) one will be based on the weak formulation

$$\langle K^{-1}\mathbf{u}, \mathbf{v}\rangle_\Omega - \langle p, \operatorname{div}\mathbf{u}\rangle_\Omega = -\langle g, \mathbf{v}\cdot\nu\rangle_{\partial\Omega} \qquad \forall \mathbf{v} \in H(\operatorname{div}, \Omega), \tag{5}$$

$$\langle \operatorname{div}\mathbf{u}, q\rangle_\Omega = \langle f, q\rangle_\Omega \qquad \forall q \in L^2(\Omega). \tag{6}$$

Here ν is a unit outward normal to the boundary $\partial\Omega$ and the bilinear forms $\langle u, v\rangle_\Omega$ and $\langle u, v\rangle_{\partial\Omega}$ stand for the integrals

$$\langle u, v\rangle_\Omega := \int_\Omega u\ v\ d\Omega \qquad \text{and} \qquad \langle u, v\rangle_\Omega := \int_{\partial\Omega} u\ v\ ds. \tag{7}$$

Let Ω_h be a tessellation of the domain Ω into polygonal elements E. Take

$$h = \max_{E\in\Omega_h} \operatorname{diam} E$$

to be a characterization of the mesh refinement. The MFD formulation will have a form similar to (5-6): find $(\mathbf{u}_h, p_h) \in X_h \times Q_h$ such that

$$[\mathbf{u}_h, \mathbf{v}_h]_{X_h} - [p_h, \mathcal{DIV}\,\mathbf{v}_h]_{Q_h} = -\langle g_h, \mathbf{v}_h\cdot\nu\rangle_h \qquad \forall \mathbf{v}_h \in X_h, \tag{8}$$

$$[\mathcal{DIV}\,\mathbf{u}_h, q_h]_{Q_h} = [f_h, q_h]_{Q_h} \qquad \forall q_h \in Q_h, \tag{9}$$

where $\mathbf{u}_h, \mathbf{v}_h, p_h$ and q_h are discrete version of $\mathbf{u}, \mathbf{v}, p$ and q. We will give a precise definition of the discrete spaces X_h and Q_h and the mimetic inner products $[\mathbf{u}_h, \mathbf{v}_h]_{X_h}$ and $[p_h, q_h]_{Q_h}$ in section 3. In fact, the definition of the discrete space Q_h will be the same as in the original method [1]. Next we will discuss the changes from the original method.

2.1 Changes to the flux DoF

The original method described in [1] uses *degrees of freedom* for flux defined on each element $E \in \Omega_h$ and on each edge $e \in \partial E$. Their number depends on the order of the scheme k. In this project we remove two DoFs from each edge e and move them to the vertices. Thus each vertex now has two DoFs associated with it. These DoFs are simply the x- and y-components of the flux at this vertex.

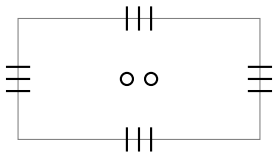

Figure 1: Flux degrees of freedom for original method on a quadrilateral element ($k = 2$)

Choose $k \in \mathbb{N}$ that represents the order of MFD method, fix $E \in \Omega_h$ and let $\mathcal{E}_E$ be the set of all edges of E and $\mathcal{V}_E$ be the set of all vertices of E. Then the DoFs of flux $\mathbf{u}$ on E are defined as

- the moments of $\mathbf{u}$ with respect to $\nabla\phi_{E,i}$ where $\{\phi_{E,i}\}_i$ is the basis of $\mathcal{P}_{k-1}(E)$, the space of all polynomials on E with degree less or equal to $k-1$:

$$u^I_{E,i} := \frac{1}{|E|}\int_E \langle \mathbf{u}, \nabla\phi_{E,i}\rangle dx \quad \text{for } i = 1, \dots, n^E_{k-1}; \tag{10}$$

  Here we skip the first constant polynomial since the gradient turns it into zero. For the sake of simplicity of implementation we take $\phi_{E,i} = x^{\alpha_1} y^{\alpha_2}$ where i indexes the power $\alpha = (\alpha_1, \alpha_2)$.

- the moments of $\mathbf{u}\cdot\nu_{E,e}$ with respect to $\phi_{e,i}$, where $\nu_{E,e}$ is the unit outward normal to the element E at the edge e and $\{\phi_{e,i}\}_{i=0}^k$ is the *orthogonal* basis of $\mathcal{P}_k(e)$ - polynomials of degree up to k on e:

$$u^I_{e,i} := \frac{1}{|e|}\int_e \langle \mathbf{u}, \nu_{E,e}\rangle \phi_{e,i}(s) ds \quad \text{for } i = 2, \dots, k \quad \forall e \in \mathcal{E}_E; \tag{11}$$

  We take orthogonal Legendre polynomials as $\phi_{e,i}$. Here we skip the first two polynomials 1 and s since the coefficients in front of them can be determined through the vertex DoFs.

- the values of $\mathbf{u}$ at the vertices of E:

$$\mathbf{u}^I_v := \mathbf{u}|_v \quad \forall v \in \mathcal{V}_E. \tag{12}$$

  Note, that $\mathbf{u}^I_v = (u^I_{v,1}, u^I_{v,2})$ is a vector and contains two scalar DoFs.

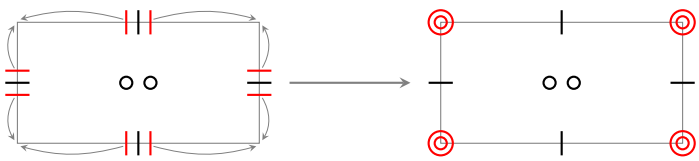

Figure 2: Change of the flux degrees of freedom for new method on a quadrilateral element ($k = 2$)

The DoFs of a scalar function p on E are defined as

- the polynomial coefficients of the projection $\Pi^E_{k-1}p$ of the function p on space $\mathcal{P}_{k-1}$ of polynomials of order up to $k-1$:

$$\Pi^E_{k-1}p = \sum_{i=0}^{n^E_{k-1}} p^I_{E,i}\phi_{E,i}, \tag{13}$$

  where $\phi_{E,i} = x^{\alpha_i} y^{\beta_i}$ are the monomials that form the basis of $\mathcal{P}_{k-1}$.

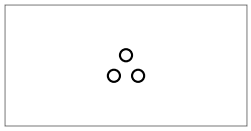

Figure 3: Degrees of freedom for potential on a quadrilateral element ($k = 2$)

The local change of DoFs shown on Figure 2 is a one-to-one correspondence T_E as soon as E does not have hanging nodes, that are the vertices with parallel incident edges. Such approach was used at the beginning and the matrix T_E was calculated for each element $E \in \Omega_h$ so that

$$T_E \mathbf{u}^I_{old} = \mathbf{u}^I_{new}. \tag{14}$$

Later the more detailed approach was used where all flux DoFs were found independently of the original method. This approach is discussed in Section 3.

Despite the local change of DoFs is one-to-one for elements with no hanging nodes, globally the number of DoFs decreases (Figure 4).

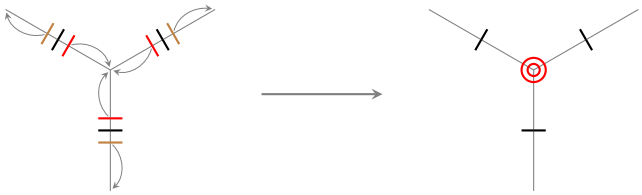

Figure 4: Change of the flux degrees near single node

The number of DoFs near one node is decreased by the number of incident edges and increased by two. Figure 5 shows the global decrease of number of DoFs for a regular square mesh.

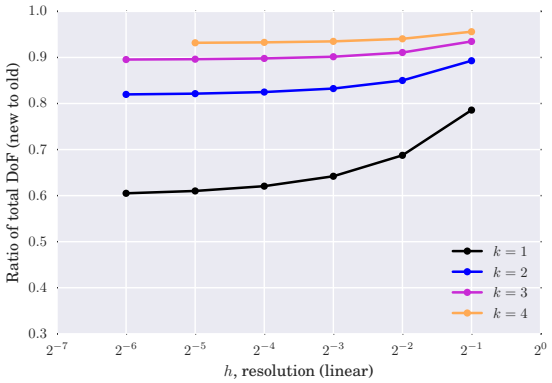

Figure 5: Ratio of number of new DoFs to number of old DoFs

Another difference between two methods is that the new method has additional continuity of the flux at the vertices (Figure 6) since vertex DoFs match with DoFs on incident edges.

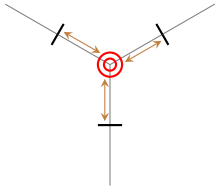

Figure 6: Flux is continuous at the vertices

This brings additional properties for the discrete approximation but also creates additional difficulties when dealing with the problems with discontinuous diffusion coefficient. The actual analytical solution for such problems has a continuous normal component across the edges of discontinuity but its tangential component can have jumps that our model does not allow. Therefore the discontinuous diffusion coefficient case requires special consideration.

3 Discretization of bilinear forms

To solve the problem (8)-(9) we need to describe the discrete divergence operator $\mathcal{DIV}$ and the mimetic inner products $[\cdot,\cdot]_{X_h}$ and $[\cdot,\cdot]_{Q_h}$ that are the bilinear forms on the corresponding vector spaces. The bilinear forms correspond to some symmetric positive definite matrices $\mathcal{M}_{X_h}$ and $\mathcal{M}_{Q_h}$:

$$[\mathbf{u},\mathbf{v}]_{X_h} = \mathbf{u}^T \mathcal{M}_{X_h} \mathbf{v}, \tag{15}$$

$$[p,q]_{Q_h} = p^T \mathcal{M}_{Q_h} q, \tag{16}$$

where $\mathbf{u},\mathbf{v} \in X_h$ and $p,q \in Q_h$ are represented as column vectors collecting all their DoF. Our job is to find $\mathcal{DIV}$, $\mathcal{M}_{X_h}$, and $\mathcal{M}_{Q_h}$. We fix element $E \in \Omega_h$ and construct the local matrices $\mathcal{DIV}_E$, $\mathcal{M}_{X_E}$, and $\mathcal{M}_{Q_E}$. The global matrices are then constructed additively.

The bilinear form for the scalar variable $\mathcal{M}_{Q_E}$ is constructed in the same way as in [1] since the scalar moments $p^I_{E,i}$ are not changed. It contains all pairwise L^2-inner products of basis monomials $\phi_{E,i}$. If p and q are scalar functions on E, then

$$\begin{aligned}[p^I,q^I]_{Q_E} :&= \int_E \Pi^E_{k-1} p \cdot \Pi^E_{k-1} q \, dx = \int_E \sum_i p^I_{E,i}\phi_{E,i} \cdot \sum_j q^I_{E,j}\phi_{E,j} dx \\ &= \sum_{i,j} p^I_{E,i}\, q^I_{E,j}\, (\mathcal{M}_{Q_E})_{ij} = \left(p^I\right)^T \mathcal{M}_{Q_E} q^I \end{aligned} \tag{17}$$

where

$$(\mathcal{M}_{Q_E})_{ij} = \int_E \phi_{E,i}\phi_{E,j} dx. \tag{18}$$

Instead of the discrete divergence operator we consider the combination of $\mathcal{M}_{Q_h}$ with $\mathcal{DIV}_E$ and describe $[\mathcal{DIV}_E\, \mathbf{u}^I, p^I]_{Q_h}$ with $p \in \mathcal{P}_{k-1}(E)$ as an action of some operator on the discrete representation $\mathbf{u}^I$ of $\mathbf{u}$. The coordinates of the vector $\mathbf{u}^I$ are simply the DoFs of $\mathbf{u}$ associated with the element E. This includes DoFs associated with verteces and edges of the element E as well as those associated with the area of the element. To understand how $[\mathcal{DIV}_E\, \mathbf{u}^I, p^I]_{Q_h}$ is represented through the DoFs of $\mathbf{u}$ for any polynomial $p \in \mathcal{P}_k(E)$, we test it on all basis monomials $\phi_{E,i} = x^{\alpha_1} y^{\alpha_2}$ with $|\alpha| \le k-1$. By definition

$$\begin{aligned}[\mathcal{DIV}_E\, \mathbf{u}^I, \phi_{E,i}]_{Q_h} &= [(\operatorname{div}\mathbf{u})^I, \phi_{E,i}]_{Q_h} = \int_E \operatorname{div}\mathbf{u} \cdot \phi_{E,i} dx \\ &= -\int_E \mathbf{u}\cdot\nabla\phi_{E,i} dx + \sum_{e\in\mathcal{E}_E} \int_e \langle \mathbf{u}, \nu_{E,e}\rangle \phi_{E,i} ds \\ &= -u^I_{E,i} + \frac{1}{|E|} \sum_{e\in\mathcal{E}_E} \int_e \langle \mathbf{u}, \nu_{E,e}\rangle \phi_{E,i} ds. \end{aligned} \tag{19}$$

Now fix $e \in \mathcal{E}_E$ and calculate $\int_e \langle \mathbf{u}, \nu_{E,e}\rangle \phi_{E,i} ds$. Both the monomial $\phi_{E,i}$ and polynomial $\langle \mathbf{u}, \nu_{E,e}\rangle$ can be represented through the Legendre basis on the edge e (for simplicity we skip the dependence on E, i, and e)

$$\phi_{E,i} = \sum_{j=0}^k p_j \phi_{e,j} \quad \text{and} \quad \langle \mathbf{u}, \nu_{E,e}\rangle = \sum_{j=0}^k q_j \phi_{e,j}. \tag{20}$$

Then

$$\begin{aligned}\int_e \langle \mathbf{u}, \nu_{E,e}\rangle \phi_{E,i} ds &= \int_e \langle \mathbf{u}, \nu_{E,e}\rangle \sum_{j=0}^k p_j \phi_{e,j} ds \\ &= |e| \sum_{j=2}^k p_j u^I_{e,j} + \frac{|e|}{2} \int_{-1}^1 (q_0\phi_{e,0} + q_1\phi_{e,1})(a_0\phi_{e,0} + p_1\phi_{e,1})\, dt \\ &= |e| \sum_{j=2}^k p_j u^I_{e,j} + \frac{|e|}{2} \left[2q_0p_0 + \frac{2}{3} q_1 p_1 \right]. \end{aligned} \tag{21}$$

The only unknowns here are q_0 and q_1 and we want to represent them through edge DoFs $u^I_{e,j}$, $j = 2, \dots, k$ and vertex DoFs $\mathbf{u}^I_{v_1}$ and $\mathbf{u}^I_{v_2}$, where v_1 and v_2 are the adjacent to e vertices.

For simplicity we start with *auxiliary* DoFs instead of $\mathbf{u}^I_{v_1}$ and $\mathbf{u}^I_{v_2}$ that are their normal components w.r.t. $\nu_{E,e}$:

$$\langle \mathbf{u}^I_{v_1}, \nu_{E,e} \rangle = \langle \mathbf{u}, \nu_{E,e} \rangle\big|_{v_1} = u^A_{v_1,2} \quad \text{and} \quad \langle \mathbf{u}^I_{v_2}, \nu_{E,e} \rangle = \langle \mathbf{u}, \nu_{E,e} \rangle\big|_{v_2} = u^A_{v_2,1}. \tag{22}$$

Since the rescaled Legendre polynomials $\phi_{e,j}(t)$ on $[-1, 1]$ take value 1 at $t = 1$ and alternate between -1 and 1 at $t = -1$, we can write the system for q_0 and q_1:

$$u^A_{v_1,2} = \langle \mathbf{u}, \nu_{E,e} \rangle\big|_{v_1} = \sum_{j=0}^{k} q_j \phi_{e,j}(-1) = q_0 - q_1 + q_2 - \dots + (-1)^k q_k, \tag{23}$$

$$u^A_{v_2,1} = \langle \mathbf{u}, \nu_{E,e} \rangle\big|_{v_2} = \sum_{j=0}^{k} q_j \phi_{e,j}(1) = q_0 + q_1 + q_2 + \dots + q_k. \tag{24}$$

The coefficients q_i, $i \geq 2$ are simply the edge DoFs up to some factor:

$$\begin{aligned} u^I_{e,i} &= \frac{1}{|e|} \int_e \langle \mathbf{u}, \nu_{E,e} \rangle \phi_{e,i} ds = \frac{1}{|e|} \int_e \sum_{j=0}^{k} q_j \, \phi_{e,j} \phi_{e,i} ds \\ &= \frac{q_i}{|e|} \cdot \frac{|e|}{2} \int_{-1}^{1} (\phi_{e,i})^2 \, ds = \frac{q_i}{2} \cdot \frac{2}{2i+1} = \frac{1}{2i+1} \, q_i. \end{aligned} \tag{25}$$

Therefore we can express q_0 and q_1 through edge DoFs $u^I_{e,i}$ and auxiliary vertex DoFs $u^A_{v,j}$:

$$q_0 = \frac{u^A_{v_2,1} + u^A_{v_1,2}}{2} - \sum_{l=1}^{\lfloor \frac{k}{2} \rfloor} (4l+1) u^I_{e,2l} \,, \tag{26}$$

$$q_1 = \frac{u^A_{v_2,1} - u^A_{v_1,2}}{2} - \sum_{l=1}^{\lfloor \frac{k-1}{2} \rfloor} (4l+3) u^I_{e,2l+1} \,. \tag{27}$$

Finally, using (22) and (26)-(27) we able to rewrite the edge integral as a linear combination of the edge and original vertex DoFs:

$$\begin{aligned} \int_e \langle \mathbf{u}, \nu_{E,e} \rangle \phi_{E,i} ds = |e| \Bigg[&\left(\frac{1}{2} p_0 - \frac{1}{6} p_1 \right) \langle \mathbf{u}^I_{v_1}, \nu_{E,e} \rangle + \left(\frac{1}{2} p_0 + \frac{1}{6} p_1 \right) \langle \mathbf{u}^I_{v_2}, \nu_{E,e} \rangle \\ &+ \sum_{j=2}^{k} \big(p_j - (2j+1) \alpha_j \big) u^I_{e,j} \Bigg] \end{aligned} \tag{28}$$

where

$$\alpha_j = \begin{cases} p_0, & \text{when } j \text{ is even}, \\ \frac{1}{3} p_1, & \text{when } j \text{ is odd}. \end{cases} \tag{29}$$

The equations (19) and (28) allow us to express the action of discrete divergence operator on $\mathbf{u}^I$ through the DoFs of $\mathbf{u}$ and represent it as a matrix $\mathcal{D}_E$ of size $n^s_k \times n^v_k$ where n^s_k is the number of scalar DoFs and n^v_k is the number of vector DoFs on element E. Thus, we can write

$$[\mathcal{DIV}_E \, \mathbf{u}^I, p]_{Q_E} = \big(p^I \big)^T \mathcal{D}_E \mathbf{u}^I. \tag{30}$$

The right hand side of (8) is the sum of the integrals over all boundary edges:

$$\langle g_h, \mathbf{v}_h \cdot \nu \rangle_h = \sum_{e \in \partial \Omega_h} \int_e \langle \mathbf{v}_h, \nu_e \rangle g_h ds \tag{31}$$

and can be calculated by (28)-(29) using the Legendre coefficients of g_h with respect to the basis $\{\phi_{e,j}\}_{j=0}^{k}$.

Finally, we construct the bilinear form for the vector variable $\mathcal{M}_{X_h}$. The *local consistency* condition states that for any $q \in \mathcal{P}_{k+1}(E)$ and any vector function $\mathbf{v}$ on E the following holds:

$$[\left(\Pi_k^E(K\nabla q)\right)^I, \mathbf{v}^I]_{X_E} = \int_E \langle \nabla q, \mathbf{v}\rangle dx, \tag{32}$$

i.e. the bilinear form is equivalent to integration for polynomials of order up to $k+1$. We test (32) on all monomials of order up to $k+1$. If $q = \phi_{E,j}$ is a monomial of order less or equal than $k-1$, then $\int_E \langle \nabla \phi_{E,j}, \mathbf{v}\rangle dx$ is simply the face DoF of $\mathbf{v}$ multiplied by $|E|$. In the other case we use the divergence theorem to calculate the right hand side:

$$\begin{aligned}\int_E \langle \nabla q, \mathbf{v}\rangle dx &= -\int_E q\, \Pi_{k-1}^E \mathrm{div}\, \mathbf{v}\, dx + \sum_{e\in E}\int_e \langle \mathbf{v}, \nu_{E,e}\rangle q\, ds \\ &= -\left(\mathbf{v}^I\right)^T \mathcal{D}_E^T\, q^I + \sum_{e\in E}\sum_j q_{E,j}^I \int_e \langle \mathbf{v}, \nu_{E,e}\rangle \phi_{E,j}\, ds \end{aligned} \tag{33}$$

The edge integrals in (33) can be calculated by (28) as an inner product of $\mathbf{v}^I$ with some vector c_j. Then the formula (33) can be written in a vector form:

$$\int_E \langle \nabla \phi_{E,j}, \mathbf{v}\rangle dx = \left(\mathbf{v}^I\right)^T \left(-\mathcal{D}_E^T \left(\phi_{E,j}\right)^I + c_j\right) \tag{34}$$

for all $\phi_{E,j} \in \mathcal{P}_{k+1}(E)$. We introduce the matrix of coefficients in the right hand side for all test functions $\phi_{E,j}$:

$$\mathcal{R} = [\mathcal{R}_j]_{j=1}^{n_{k+1}^E} := \left[-\mathcal{D}_E^T \left(\phi_{E,j}\right)^I + c_j\right]_{j=1}^{n_{k+1}^E}. \tag{35}$$

On the other hand, the integral on the left is the bilinear form

$$\int_E \langle \nabla \phi_{E,j}, \mathbf{v}\rangle dx = \left(\mathbf{v}^I\right)^T \mathcal{M}_{X_E} \left(\Pi_k^E(K\nabla\phi_{E,j})\right)^I. \tag{36}$$

We define the matrix of discrete representations of all $\Pi_k^E(K\nabla\phi_{E,j})$ as $\mathcal{N}$:

$$\mathcal{N} = [\mathcal{N}_j]_{j=1}^{n_{k+1}^E} := \left[\left(\Pi_k^E(K\nabla\phi_{E,j})\right)^I\right]_{j=1}^{n_{k+1}^E}. \tag{37}$$

The matrices $\mathcal{R}$ and $\mathcal{N}$ can be directly calculated and since the equations (34) and (36) hold for any vector function $\mathbf{v}$ on E, we deduce that the matrix $\mathcal{M}_{X_E}$ satisfies

$$\mathcal{M}_{X_E}\mathcal{N} = \mathcal{R}. \tag{38}$$

Thus we obtained the *local consistency* condition in a matrix form. In order to satisfy *consistency* and *stability* conditions (see [1]), the matrix $\mathcal{M}_{X_E}$ is constructed by the standard formula for mimetic inner product:

$$\mathcal{M}_{X_E} = \mathcal{M}_0 + \mathcal{M}_1 = \mathcal{R}\left(\mathcal{N}^T\mathcal{R}\right)^{-1}\mathcal{R}^T + \mu_E\left(I - \mathcal{N}\left(\mathcal{N}^T\mathcal{N}\right)^{-1}\mathcal{N}^T\right), \tag{39}$$

where the matrix $\mathcal{M}_0$ is responsible for consistency and the matrix $\mathcal{M}_1$ is responsible for stability. Note, that the matrix $\mathcal{N}^T\mathcal{R}$ is a Gram matrix for inner products between $\nabla\phi_{E,i}$ and $\nabla\phi_{E,j}$, so it is symmetric and positive definite, and therefore invertible. Thus, the formula (39) is well-defined.

4 Numerical Results

We tested the new method in comparisson with the original method on a square domain $\Omega = [0, 1]^2$ with a variety of polygonal meshes (Figure 7).

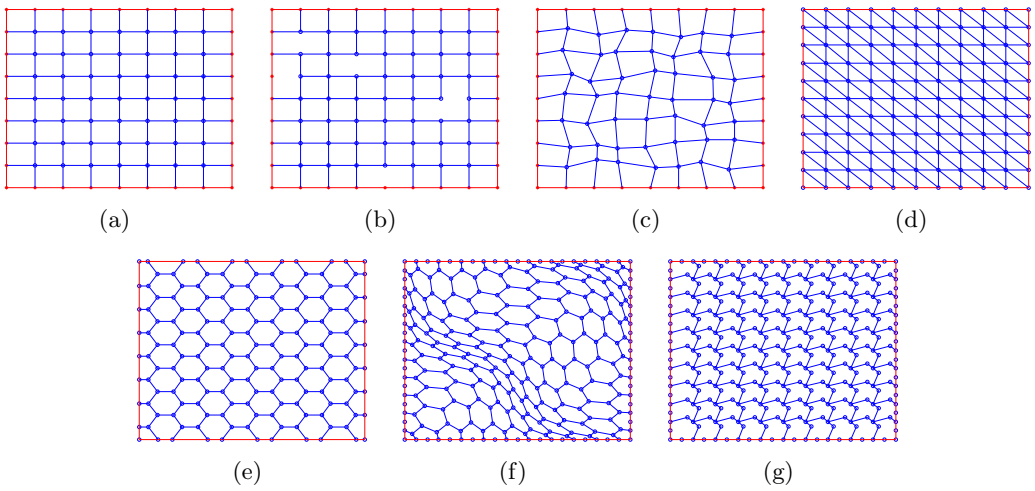

Figure 7: Meshes

The results below were calculated on a perturbed square mesh, see Figure 7c, with various degree of refinement for the tensor diffusion coefficient

$$K = \begin{bmatrix} 2 + x^2 & 0 \\ 0 & 2 + y^2 \end{bmatrix} \tag{40}$$

and the potential $p(x, y) = \sin \pi x \cos \pi y$ with the prescribed exact Dirichelet boundary conditions.

Variable	Old method error	New method error
Flux	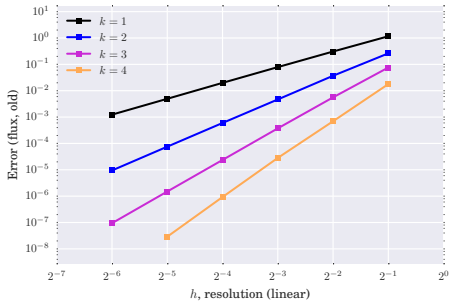	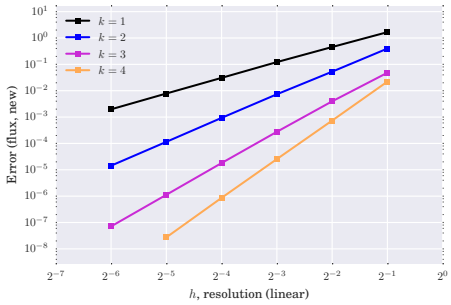
Potential	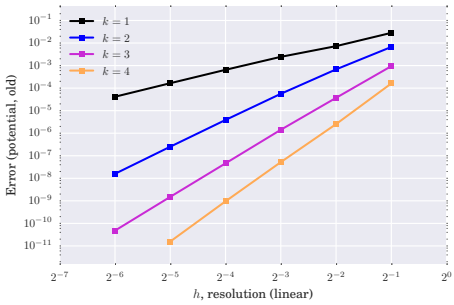	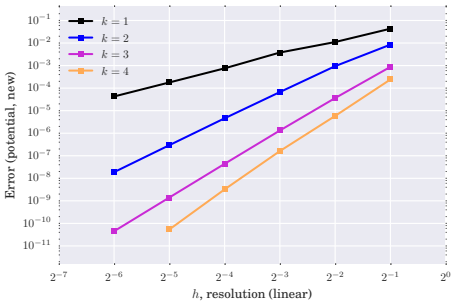

Table 1: Error comparison

The errors for the flux $\mathbf{u}^I$ and the potential p^I are comparable to the errors in the previous method that does not use vertex DoFs (see, Table 1). Similar results are obtained for other types of meshes, such as square meshes with removed edges (Figure 7b), regular hexagonal (Figure 7e), deformed hexagonal (Figure 7f), and non-convex octagonal meshes (Figure 7g). Table 2 and Table 3 illustrate the errors for the flux $\mathbf{u}^I$ and potential p^I, respectively. The results are very similar for all test meshes that we used.

Mesh	Error (flux)	Convergence rate (flux)
Square mesh with removed edges	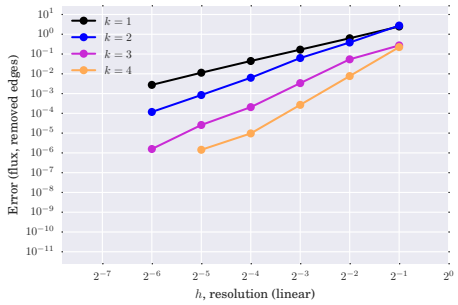	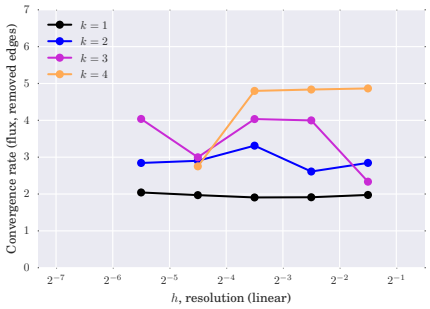
Regular hexagonal mesh	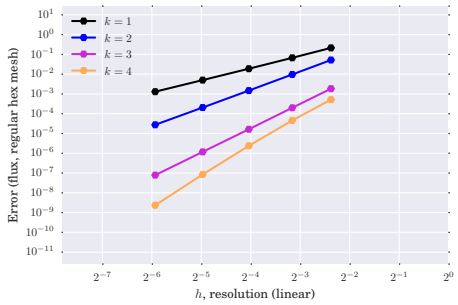	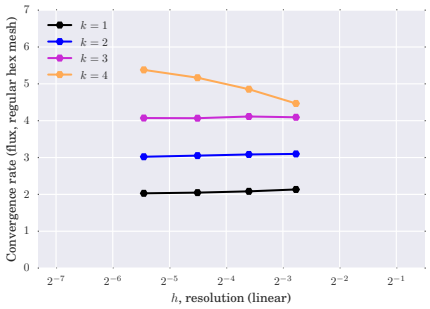
Deformed hexagonal mesh	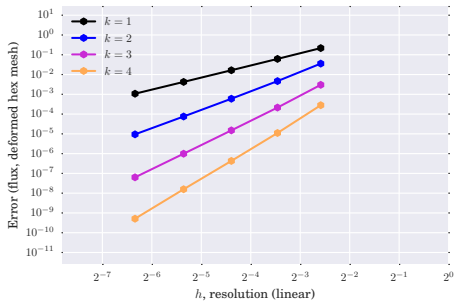	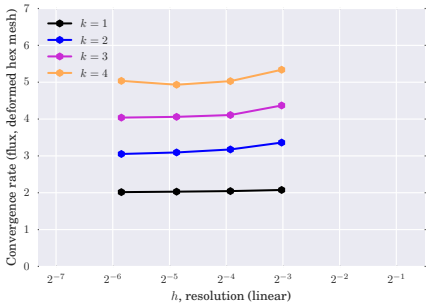
Non-convex octagonal mesh	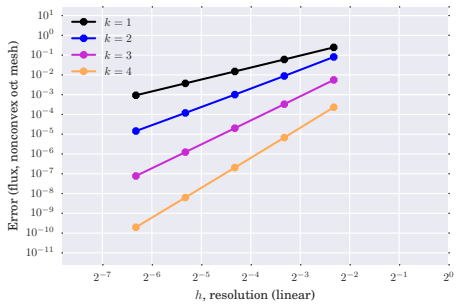	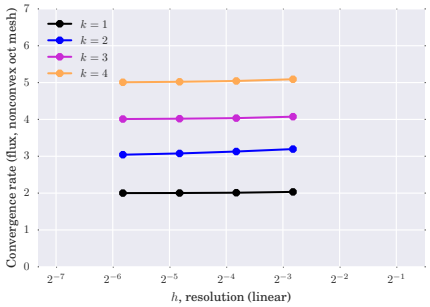

Table 2: Flux error comparison for different meshes

Mesh	Error (potential)	Convergence rate (potential)
Square mesh with removed edges	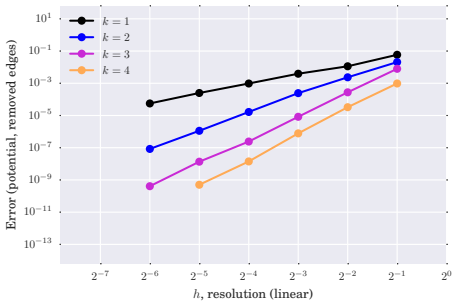	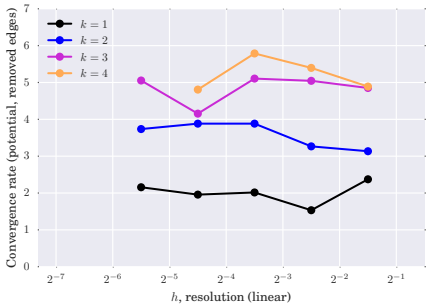
Regular hexagonal mesh	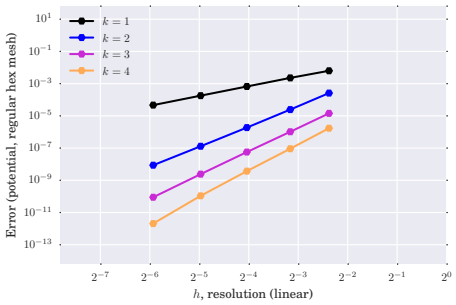	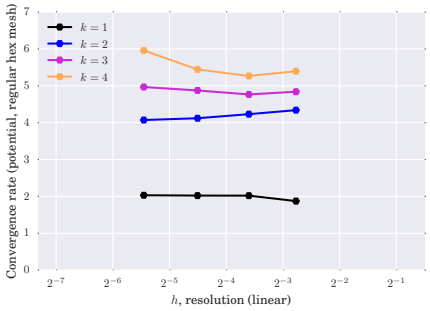
Deformed hexagonal mesh	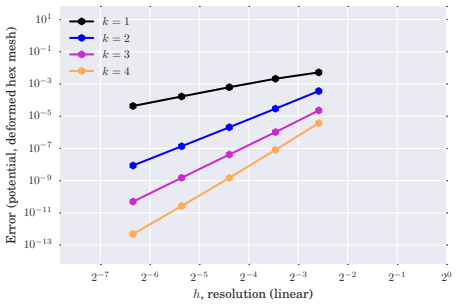	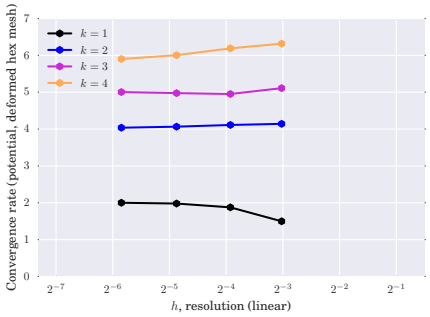
Non-convex octagonal mesh	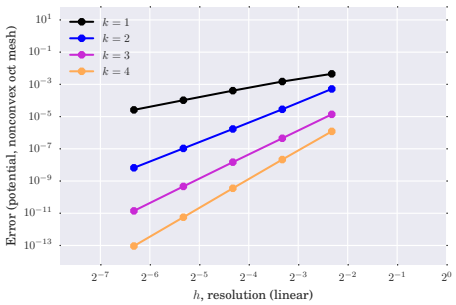	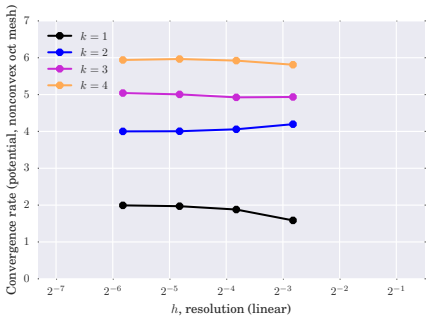

Table 3: Potential error comparison for different meshes

The convergence rates obtained experimentally (Table 2 and Table 3, third column) are $k+1$ for the flux and $k+2$ for potential when $k \geq 2$. In the case $k = 1$ the potential converges with the rate $k+1$. Thus we observe the *superconvergence* effect for p^I in the high-order schemes with $k \geq 2$.

Table 4 shows the condition number of the global coefficient matrix of the overall linear system. The plots show that condition number does not grow much for a fixed order k for different meshes, that means that the new DoFs are independent variables and the system is well-posed.

Method	Mesh	Condition number
Old	Perturbed square mesh	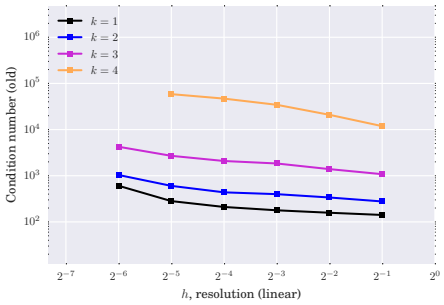
New	Perturbed square mesh	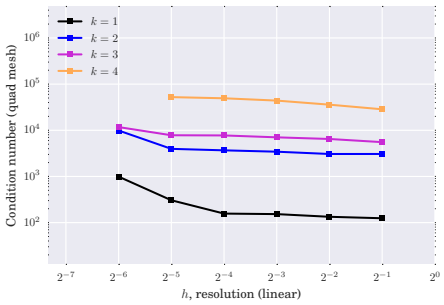
	Regular hexagonal mesh	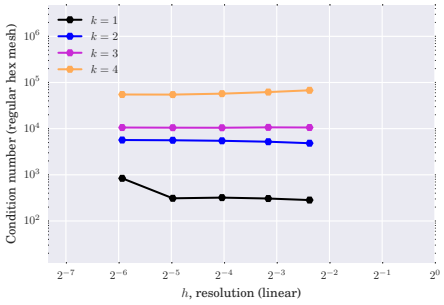
	Deformed hexagonal mesh	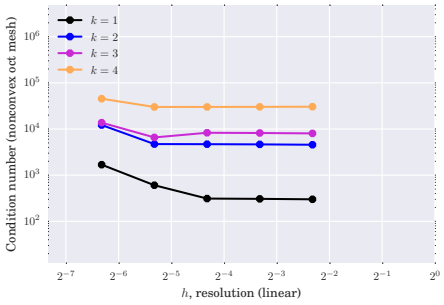

Table 4: Condition number comparison for different methods and meshes

5 Conclusion

As was demonstrated by a number of numerical experiments the new method retains all the same properties of the original method [1], such as the convergence rate both for the flux and the potential; it works equally well on structured and unstructured general polygonal meshes. At the same time the number of degrees of freedom in the new method is significantly less compared to the original method: up to 40% in the low-order case and up to $10 - 18\%$ in the high-order cases.

The added continuity in the new method did not manifest itself through any added convergence rates. It would be interesting to identify the problems where this continuity would be beneficial or even crucial.

The added continuity presented some challenges in the cases when the diffusion coefficient is discontinuous. In these cases the new method is enforcing the tangential continuity of flux variable at the interface, where such continuity is not present in the solution. As a result the new method experiences critical convergence rate loss. An idea for fixing this apparent problem is to introduce additional degrees of freedom at the interface vertices. These degrees of freedom would quantify the jump in the tangential component of the flux and therefore will remove the continuity restriction (only on the interface). The preliminary results we obtained for this problem are promising, but they cannot yet be attached to this report.

Acknowledgement

This work was performed under the auspices of the National Nuclear Security Administration of the US Department of Energy at Los Alamos National Laboratory under Contract No. DE-AC52-06NA25396. The authors gratefully acknowledge the support of the U.S. Department of Energy, National Nuclear Security Administration, Advanced Simulation and Computing (ASC) Program for the first author as well as the Laboratory Directed Research and Development (LDRD) program #20140270ER for the second and third authors.

References

[1] Vitaliy Gyrya, Konstantin Lipnikov, and Gianmarco Manzini. The arbitrary order mixed mimetic finite difference method for the diffusion equation. *ESAIM: Mathematical Modelling and Numerical Analysis*, 50(3):851–877, 2016.